Effects of internal pore pressure on closed-cell elastomeric foams

Oscar Lopez-Pamies [a,*], Pedro Ponte Castañeda [b,c], Martín I. Idiart [d,e]

[a] Department of Civil and Environmental Engineering, University of Illinois, Urbana-Champaign, IL 61801-2352, USA
[b] Department of Mechanical Engineering and Applied Mechanics, University of Pennsylvania, Philadelphia, PA 19104-6315, USA
[c] IMDEA Materials Institute, 28040 Madrid, Spain
[d] Departamento de Aeronáutica, Facultad de Ingeniería, Universidad Nacional de La Plata, Avda. 1 esq. 47, La Plata B1900TAG, Argentina
[e] Consejo Nacional de Investigaciones Científicas y Técnicas (CONICET), CCT La Plata, Calle 8 N° 1467, La Plata B1904CMC, Argentina

ABSTRACT

A micromechanics framework for porous elastomers with internal pore pressure (Idiart and Lopez-Pamies, 2012) is used together with an earlier homogenization estimate for elastomers containing vacuous pores (Lopez-Pamies and Ponte Castañeda, 2007a) to investigate the mechanical response and stability of closed-cell foams. Motivated by applications of technological interest, the focus is on isotropic foams made up of a random isotropic distribution of pores embedded in an isotropic matrix material, wherein the initial internal pore pressure is identical to the external pressure exerted by the environment (e.g. atmospheric pressure). It is found that the presence of internal pore pressure significantly stiffens and stabilizes the response of elastomeric foams, and hence that it must be taken into account when modeling this type of materials.

© 2012 Elsevier Ltd. All rights reserved.

1. Introduction

Because of the process of fabrication and/or environment of operation, more often than not the cavities in closed-cell porous elastomers are filled up by a gaseous substance that exerts an internal pressure on the surrounding matrix. In the low-porosity regime, this internal pressure can produce, for instance, the cavitation of elastomeric seals in high-pressure gas tanks upon rapid decompression (Gent and Tompkins, 1969; Yamabe and Nishimura, 2009; Yamabe et al., 2011). In the high-porosity regime – namely, in the context of closed-cell high-density foams – internal pore pressure is also expected to considerably affect the mechanical behavior and stability of these material systems.

Over the last decade, significant progress has been made in developing finite-strain micromechanics models for closed-cell porous elastomers which incorporate direct dependence on the constitutive behavior of the matrix material and the size, shape, and spatial distribution of the underlying pores (see, e.g. Danielsson et al., 2004; Lopez-Pamies and Ponte Castañeda, 2007a; Moraleda et al., 2007; Lopez-Pamies and Idiart, 2009). Yet, a common limitation of all these models is that they consider the pores to be vacuous, a simplifying assumption that might hinder their applicability in atmospheric (and higher) pressure conditions. In this paper, we concern ourselves with investigating the effects that

internal pore pressure can have on the mechanical behavior and stability of closed-cell elastomeric foams at large deformations. Motivated by applications of notable technological relevance such as in the cushioning and packaging industries, attention is focused on isotropic foams consisting of a random and isotropic distribution of pores embedded in an isotropic matrix.

We begin in Section 2 by formulating the elastostatics problem of a porous elastomer with internal pore pressure that is immersed in a pressurized environment and that is further deformed by externally applied loads. Following recent work by Idiart and Lopez-Pamies (2012), the macroscopic response and macroscopic stability of such a material is then expressed in terms of the response of an auxiliary porous elastomer with vacuous pores. The results of Section 2 are specialized in Section 3 to the case of isotropic foams wherein the internal pore pressure is initially identical to the external pressure of the environment (e.g. the Earth's atmosphere). For the response of the auxiliary material with vacuous pores, we make use of the model of Lopez-Pamies and Ponte Castañeda (2007a). Representative numerical results are presented and discussed for a silicone foam in Section 4 followed by some concluding remarks in Section 5.

2. Problem formulation

2.1. Initial and deformed configurations

Pressurized porous elastomers are taken here to consist of a continuous incompressible matrix containing a random

* Corresponding author. Tel.: +1 217 244 1242.
  E-mail addresses: pamies@illinois.edu (O. Lopez-Pamies), ponte@seas.edu (P.P. Castañeda), martin.idiart@ing.unlp.edu.ar (M.I. Idiart).

distribution of disconnected pores *filled* with a gaseous substance. Attention is restricted to short enough time scales for which there is no (significant) diffusion of the gas into the elastomeric matrix; in other words, the gas is assumed to remain within the pores for any given loading process.

We consider a specimen of the material that is immersed in a pressurized environment, with Cauchy pressure p_{ex}, and that occupies a domain Ω_0 in its *initial configuration*. The matrix is labeled as phase $r = 1$, while the filled pores are collectively identified as phase $r = 2$. The domains occupied by each individual phase are denoted by $\Omega_0^{(r)}$ so that $\Omega_0 = \Omega_0^{(1)} \cup \Omega_0^{(2)}$. It is assumed that the characteristic size of the pores is much smaller than the size of Ω_0, and that their spatial distribution is statistically uniform.

Material points are identified by their position vector $\mathbf{X}$ in Ω_0 relative to some fixed point O. The distribution of pores can be described by an indicator function $\theta_0(\mathbf{X})$ that takes the value 1 if the position vector $\mathbf{X}$ is in a pore, and 0 otherwise. The volume average of θ_0 over Ω_0 corresponds to the initial volume fraction of pores, or initial porosity, which we denote by

$$f_0 \doteq \frac{|\Omega_0^{(2)}|}{|\Omega_0|} = \frac{1}{|\Omega_0|} \int_{\Omega_0} \theta_0(\mathbf{X}) \, d\mathbf{X}. \tag{1}$$

Upon deformation of the solid, the position vector of a point in the *deformed configuration* Ω is specified by

$$\mathbf{x} = \chi(\mathbf{X}) \tag{2}$$

relative to some fixed point o, where χ is a one-to-one mapping from Ω_0 to Ω. We assume that χ is twice continuously differentiable, except possibly on the pores/matrix boundaries. The pointwise deformation of the matrix material is measured by the deformation gradient tensor

$$\mathbf{F}(\mathbf{X}) = \text{Grad}\,\chi(\mathbf{X}), \tag{3}$$

which must satisfy the incompressibility constraint $J \doteq \det \mathbf{F} = 1$ in $\Omega_0^{(1)}$. The initial and deformed configurations are shown schematically in Fig. 1.

2.2. The reference configuration

Following Idiart and Lopez-Pamies (2012), we describe the mechanical response of the pressurized solid in a *reference configuration* identified with the domain Ω_R occupied by the solid in its *drained* state, that is, in the absence of gas within the pores and in the absence of external pressure. Such a configuration is stress-free and corresponds to the natural state of the matrix material.

The total deformation of the solid is then decomposed into two separate deformations, as shown schematically in Fig. 2. The position vectors $\mathbf{X}$ and $\mathbf{x}$ in the initial and deformed configurations are expressed in terms of the corresponding position vectors in the reference configuration $\mathbf{X}_R$ as

$$\mathbf{X} = \chi'(\mathbf{X}_R) \quad \text{and} \quad \mathbf{x} = \chi''(\mathbf{X}_R), \tag{4}$$

where the functions χ' and χ'' are one-to-one mappings from Ω_R to Ω_0 and to Ω, respectively. The corresponding deformation gradient tensors are denoted by

$$\mathbf{F}'(\mathbf{X}_R) = \text{Grad}\,\chi'(\mathbf{X}_R) \quad \text{and} \quad \mathbf{F}''(\mathbf{X}_R) = \text{Grad}\,\chi''(\mathbf{X}_R) \tag{5}$$

and are subject to the incompressibility constraints $J' \doteq \det \mathbf{F}' = 1$ and $J'' \doteq \det \mathbf{F}'' = 1$ in $\Omega_R^{(1)}$. Here it should be emphasized that the distribution of pores in the reference configuration is not the same as that in the initial configuration, and should be described by an indicator function $\theta_R(\mathbf{X}_R)$ that depends on $\theta_0(\mathbf{X})$ and on the deformation χ'. For later use, we note also that the deformation gradients (3) and (5) are related via $\mathbf{F}'' = \mathbf{FF}'$.

2.3. Constitutive behavior of the elastomeric matrix and the gas within the pores

The elastomeric matrix is taken to be incompressible and hyperelastic. Relative to the natural reference configuration introduced above, the local stress-deformation relations for the matrix material in the initial and deformed states take then the conventional form

$$\mathbf{S}' = \frac{\partial W}{\partial \mathbf{F}}(\mathbf{F}') - q'\mathbf{F}'^{-T} \quad \text{and} \quad \mathbf{S}'' = \frac{\partial W}{\partial \mathbf{F}}(\mathbf{F}'') - q''\mathbf{F}''^{-T}, \tag{6}$$

where W stands for the stored-energy function of the matrix, $\mathbf{S}'$ and $\mathbf{S}''$ denote first Piola–Kirchhoff stress measures, and q' and q'' are Lagrange multipliers associated with the incompressibility constraints on $\mathbf{F}'$ and $\mathbf{F}''$. In view of relation $(6)_2$, it follows that the Cauchy stress $\mathbf{T}$ at each point $\mathbf{x} \in \Omega^{(1)}$ can be written as

$$\mathbf{T} = \mathbf{S}''\mathbf{F}''^T = \left[\frac{\partial W}{\partial \mathbf{F}}(\mathbf{FF}')\right]\mathbf{F}'^T\mathbf{F}^T - q''\mathbf{I}. \tag{7}$$

Making use of this last expression, we can define the first Piola–Kirchhoff stress $\mathbf{S}$ at each point $\mathbf{X} \in \Omega_0^{(1)}$ as

$$\mathbf{S} \doteq \mathbf{TF}^{-T} = \left[\frac{\partial W}{\partial \mathbf{F}}(\mathbf{FF}')\right]\mathbf{F}'^T - q''\mathbf{F}^{-T}, \tag{8}$$

which provides the nominal constitutive relation of the *pre-stressed* matrix material relative to the initial configuration.

In turn, we assume that the Cauchy internal pressure p exerted by the gas on the matrix surrounding the pores depends only on the current gas density ρ and hence write

$$p = \mathcal{P}(\rho). \tag{9}$$

The gas density in the initial configuration is further taken to be the same in all pores and is denoted by ρ_0; the initial pressure level is thus $p_0 = \mathcal{P}(\rho_0)$ in Ω_0. For calculation purposes, it proves helpful to recognize that the description (9) is equivalent to treating the gaseous substance filling the pores as an elastic fluid (see, for instance, Section 2.1.4 in the monograph by Ogden (1997)). The Cauchy stress
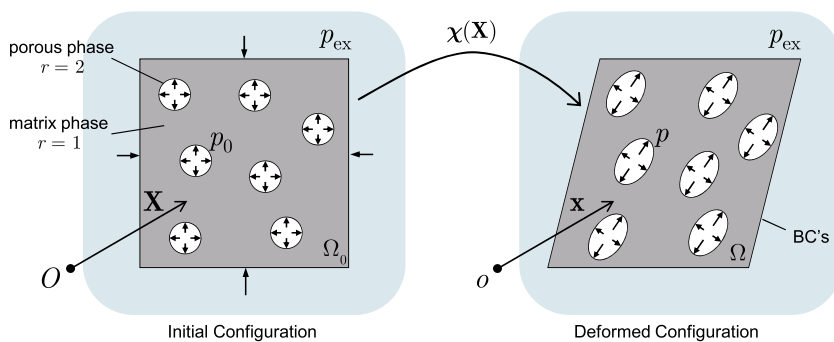

Fig. 1. Schematic of the porous elastomer with internal pore pressure in its initial and deformed configurations.
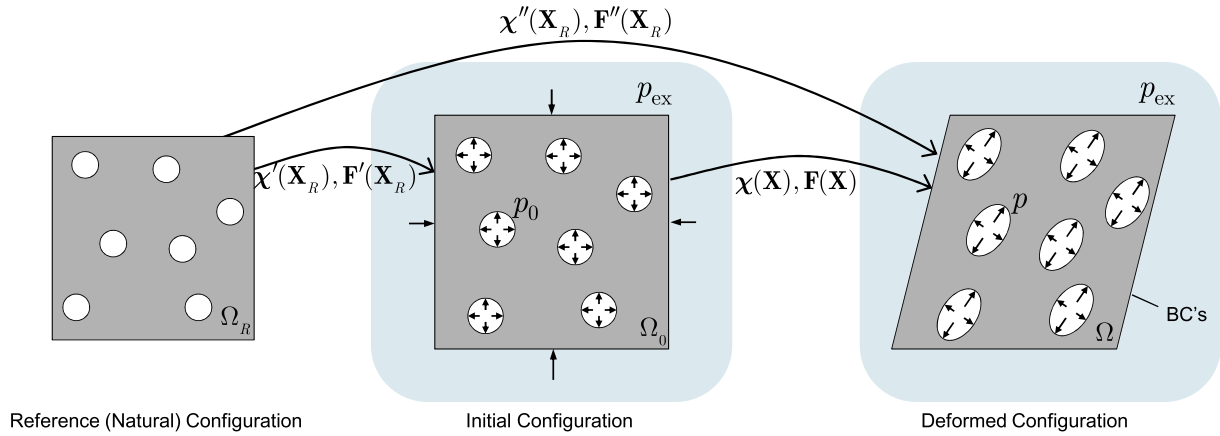
Fig. 2. Schematic of the porous elastomer and its configurations.

T can therefore be expediently defined at each point $\mathbf{x} \in \Omega^{(2)}$ – and not only on the boundary of the pores – as

$$\mathbf{T} = -p\mathbf{I} = -\mathcal{P}(J^{-1}\rho_0)\mathbf{I}, \tag{10}$$

while

$$\mathbf{S} = -pJ\mathbf{F}^{-T} = -J\mathcal{P}(J^{-1}\rho_0)\mathbf{F}^{-T} \tag{11}$$

defines the nominal pressure at each $\mathbf{X} \in \Omega_0^{(2)}$.

2.4. Macroscopic response and stability

Granted the hypothesis of separation of length scales and statistical uniformity, the overall or macroscopic response of the above-introduced pressurized solid can be defined as the relation between the volume averages of the first Piola–Kirchoff stress **S** and the deformation gradient **F** over the volume Ω_0 when the specimen is subjected to the affine boundary condition

$$\chi = \overline{\mathbf{F}}\mathbf{X} \quad \text{on } \partial\Omega_0, \tag{12}$$

with the second-order tensor $\overline{\mathbf{F}}$ denoting a prescribed quantity (Hill, 1972). In this case, it directly follows from the divergence theorem that the average deformation gradient over Ω_0 is given by $|\Omega_0|^{-1} \int_{\Omega_0} \mathbf{F}(\mathbf{X}) \, d\mathbf{X} = \overline{\mathbf{F}}$, and hence the derivation of the macroscopic response reduces to finding the average stress $\overline{\mathbf{S}} \doteq |\Omega_0|^{-1} \int_{\Omega_0} \mathbf{S}(\mathbf{X}) \, d\mathbf{X}$ for a given $\overline{\mathbf{F}}$, namely, the relation

$$\overline{\mathbf{S}} = \mathcal{S}(\overline{\mathbf{F}}; \theta_0), \tag{13}$$

where the dependence on the microstructure has been made explicit for clarity. For later use, we also recall (Hill, 1972) that the average Cauchy stress over the deformed configuration Ω can be written in terms of (13) simply as

$$\overline{\mathbf{T}} \doteq \frac{1}{|\Omega|} \int_\Omega \mathbf{T}(\mathbf{x}) d\mathbf{x} = \frac{1}{\overline{J}} \mathcal{S}(\overline{\mathbf{F}}; \theta_0)\overline{\mathbf{F}}^T, \tag{14}$$

where $\overline{J} \doteq \det \overline{\mathbf{F}}$.

As shown by Idiart and Lopez-Pamies (2012), it is possible to expediently write the macroscopic response function $\mathcal{S}$ of the pressurized solid in terms of the macroscopic response function of the drained solid,[1] denoted here by $\widetilde{\mathcal{S}}$. The result reads as follows

$$\mathcal{S}(\overline{\mathbf{F}}; \theta_0) = \frac{1}{\overline{J}'} \widetilde{\mathcal{S}}(\overline{\mathbf{F}}\overline{\mathbf{F}}'; \theta_R)\overline{\mathbf{F}}'^T - \overline{\mathcal{P}}(\overline{J})\overline{J}\overline{\mathbf{F}}^{-T}, \tag{15}$$

where $\overline{\mathcal{P}}(\overline{J}) \doteq \mathcal{P}(\rho_0 f_0/(\overline{J} - 1 + f_0))$, $\overline{J}' \doteq \det \overline{\mathbf{F}}'$, $\overline{\mathbf{F}}'$ is solution to

$$\widetilde{\mathcal{S}}(\overline{\mathbf{F}}'; \theta_R) = (p_0 - p_{ex})\overline{J}'\overline{\mathbf{F}}'^{-T}, \tag{16}$$

and the macroscopic response of the drained solid is determined by the standard homogenization problem

$$\widetilde{\mathcal{S}}(\overline{\mathbf{F}}; \theta_R) = \frac{\partial \widetilde{W}}{\partial \overline{\mathbf{F}}}(\overline{\mathbf{F}}; \theta_R) \quad \text{with}$$

$$\widetilde{W}(\overline{\mathbf{F}}; \theta_R) = \min_{\mathbf{F}'' \in \mathcal{K}(\overline{\mathbf{F}})} \frac{1}{|\Omega_R|} \int_{\Omega_R} [1 - \theta_R(\mathbf{X}_R)]W(\mathbf{F}'')d\Omega_R. \tag{17}$$

Thus, the computation of the macroscopic response function (15) for a porous elastomer with initial internal pore pressure p_0, that is immersed in a pressurized environment with pressure p_{ex}, amounts to solving the algebraic Eq. (16) together with the conventional homogenization problem (17) for a porous elastomer with *vacuous* pores in a *vacuous* environment, where the matrix material is initially in its stress-free (natural) state. Note that when $p_0 = p_{ex} = 0$, $\overline{\mathcal{P}}(\overline{J}) = 0$, the reference and initial configurations coincide ($\theta_0' = \theta_0$), $\overline{\mathbf{F}}' = \mathbf{I}$ is solution to Eq. (16) and $\mathcal{S}$ reduces to $\widetilde{\mathcal{S}}$.

In addition to characterizing the macroscopic constitutive response, the above formulation can provide information about the onset of macroscopic instabilities, that is, geometric instabilities with wavelengths much larger than the characteristic size of the pores (Geymonat et al., 1993; Michel et al., 2007). In particular, it can be shown that the pressurized solid may become macroscopically unstable whenever the condition

$$\min_{\|\mathbf{u}\|=\|\mathbf{v}\|=1} Q(\overline{\mathbf{F}}; \theta_0, \mathbf{u}, \mathbf{v}) = 0 \tag{18}$$

with

$$Q(\overline{\mathbf{F}}; \theta_0, \mathbf{u}, \mathbf{v}) = \overline{F}_{jp}\overline{F}_{lq} \frac{\partial \mathcal{S}_{kq}}{\partial \overline{F}_{ip}}(\overline{\mathbf{F}}; \theta_0)u_j u_l v_i v_k \tag{19}$$

is first satisfied along an arbitrary loading path with starting point $\overline{\mathbf{F}} = \mathbf{I}$.

2.5. The case of $p_0 = p_{ex}$

For the physically relevant case when the initial pressure within the pores p_0 is identical to the externally applied pressure p_{ex} – to be the focus of our analysis subsequently – the solution to Eq. (16) is simply given by $\overline{\mathbf{F}}' = \mathbf{I}, \theta_0' = \theta_0$, and hence the macroscopic response (15) of the pressurized solid reduces to

$$\mathcal{S}(\overline{\mathbf{F}}; \theta_0) = \frac{\partial \widetilde{W}}{\partial \overline{\mathbf{F}}}(\overline{\mathbf{F}}; \theta_0) - \overline{\mathcal{P}}(\overline{J})\overline{J}\overline{\mathbf{F}}^{-T} \tag{20}$$

---

[1] Upon deformation, the internal pressure in a given pore will depend on the volume change of that pore. In a general deformation process each pore will grow differently and therefore a non-uniform internal pressure p will develop. The procedure of Idiart and Lopez-Pamies (2012) relies on the assumption that the pore pressure p remains uniform. While an approximation, this assumption turns out to be exact if the homogenization theory utilized for the drained solid predicts uniform mechanical fields in the pores. This is the case of all the theories mentioned in Section 1.

with

$$\widetilde{W}(\overline{\mathbf{F}};\theta_0) = \min_{\mathbf{F}\in\mathcal{K}(\overline{\mathbf{F}})} \frac{1}{|\Omega_0|} \int_{\Omega_0} [1-\theta_0(\mathbf{X})]W(\mathbf{F})\mathrm{d}\Omega_0. \tag{21}$$

In turn, the stability condition (18) specializes to

$$\min_{\|\mathbf{u}\|=\|\mathbf{v}\|=1}\left[\widetilde{Q}(\overline{\mathbf{F}};\theta_0,\mathbf{u},\mathbf{v}) - \overline{J}^2\frac{\mathrm{d}\overline{\mathcal{P}}}{\mathrm{d}\overline{J}}(\overline{J})(\mathbf{u}\cdot\mathbf{v})^2\right] = 0, \tag{22}$$

where

$$\widetilde{Q}(\overline{\mathbf{F}};\theta_0,\mathbf{u},\mathbf{v}) = \overline{F}_{jp}\overline{F}_{lq}\frac{\partial^2\widetilde{W}}{\partial\overline{F}_{kq}\partial\overline{F}_{ip}}(\overline{\mathbf{F}};\theta_0)u_ju_lv_iv_k. \tag{23}$$

The objective of this paper is to gain insight into the effects that internal pore pressure can have on the mechanical response and stability of closed-cell foams, as characterized by (15) and (18). Attention will be restricted to isotropic foams – made up of isotropic matrix materials and isotropic distribution of pores – wherein the internal pore pressure is equal to the external applied pressure in the initial configuration. The relevant analysis is presented in the next section, while more specific results for a silicone foam are the focus of Section 4.

3. Application to isotropic closed-cell foams

While the formulation presented in the previous section applies to matrix materials and gases within the pores characterized by arbitrary functions W and $\mathcal{P}$, in the sequel we consider the matrix to be an isotropic hyperelastic solid characterized by the stored-energy function (Lopez-Pamies, 2010)

$$W(\mathbf{F}) = \begin{cases} \frac{3^{1-\alpha_1}}{2\alpha_1}\mu_1(I_1^{\alpha_1}-3^{\alpha_1}) + \frac{3^{1-\alpha_2}}{2\alpha_2}\mu_2(I_1^{\alpha_2}-3^{\alpha_2}) & \text{if } \det\mathbf{F}=1 \\ +\infty & \text{otherwise} \end{cases}, \tag{24}$$

where $I_1 = \mathbf{F}\cdot\mathbf{F}$ and $\alpha_1,\mu_1,\alpha_2,\mu_2$ are real-valued material parameters. In turn, the gas within the pores is assumed to be an ideal gas so that

$$\mathcal{P}(\rho) = \overline{\mathcal{P}}(\overline{J}) = \frac{f_0}{\overline{J}-1+f_0}p_0. \tag{25}$$

Here, it is worth remarking that the above two constitutive choices (24) and (25) have been shown to describe reasonably well the response of a variety of elastomers and gaseous substances over large ranges of deformations. We further consider that the distribution of pores in the initial configuration is isotropic and that the initial pore pressure p_0 is identical to the external pressure p_{ex} of the environment.

In view of the above constitutive, geometric, and environment restrictions, it follows from (20) that the macroscopic response function for the foam with pressurized pores can be simply written (with a slight abuse of notation) as

$$\mathcal{S}(\overline{\mathbf{F}};f_0) = \frac{\partial\widetilde{W}}{\partial\overline{\mathbf{F}}}(\overline{\mathbf{F}};f_0) - \frac{f_0\overline{J}}{\overline{J}-1+f_0}p_0\overline{\mathbf{F}}^{-T}, \tag{26}$$

whereas the macroscopic stability condition (22) specializes to

$$\min_{\|\mathbf{u}\|=\|\mathbf{v}\|=1}\left[\widetilde{Q}(\overline{\mathbf{F}};f_0,\mathbf{u},\mathbf{v}) + \frac{f_0\overline{J}^2p_0}{(\overline{J}-1+f_0)^2}(\mathbf{u}\cdot\mathbf{v})^2\right] = 0, \tag{27}$$

where it is recalled that $\widetilde{Q}$ is given explicitly by expression (23).

To close the problem, an effective stored-energy function $\widetilde{W}$ for the auxiliary drained material is required. In this work, we make use of the result of Lopez-Pamies and Ponte Castañeda (2007a) which reads as

$$\widetilde{W}(\overline{\mathbf{F}};f_0) = (1-f_0)\left[\frac{3^{1-\alpha_1}}{2\alpha_1}\mu_1\left(\widehat{I}_1^{\alpha_1}-3^{\alpha_1}\right) + \frac{3^{1-\alpha_2}}{2\alpha_2}\mu_2\left(\widehat{I}_1^{\alpha_2}-3^{\alpha_2}\right)\right]. \tag{28}$$

Here, the variable $\widehat{I}_1 = \widehat{I}_1(\overline{\mathbf{F}};f_0)$ is given by expression (62) in Lopez-Pamies and Ponte Castañeda (2007a) in terms of the solution to a system of seven algebraic equations formed by relations (57) and (58) in Appendix C of that reference. In general, it is not possible to solve these equations in closed form, and hence $\widehat{I}_1$ must be determined numerically. For the special and physically relevant case of hydrostatic loading when $\overline{\mathbf{F}} = \overline{\lambda}\mathbf{I}$, however, the expression for $\widehat{I}_1$ reduces to the closed-form expression

$$\widehat{I}_1 = \frac{\overline{\lambda}^2}{3u^2f_0}\left[9u^2f_0 - 6uf_0\overline{\lambda}(\overline{\lambda}^3-1) + (2+f_0)\overline{\lambda}^2(\overline{\lambda}^3-1)^2\right], \tag{29}$$

where u is the root to the cubic equation

$$u^3 - \overline{\lambda}^4u^2 + \frac{1}{3f_0}(f_0-1)(\overline{\lambda}^3-1)\overline{\lambda}^5u$$
$$-\frac{1}{27f_0^{3/2}}(\sqrt{f_0}-1)^2(2+\sqrt{f_0})(\overline{\lambda}^3-1)^2\overline{\lambda}^6 = 0 \tag{30}$$

that satisfies $u = 1$ when $\overline{\lambda}=1$.

It should be plain from the above results that the macroscopic response and stability of isotropic closed-cell foams is sensitive to the internal pressure p_0 within the underlying pores. To better reveal this dependency, sample numerical results are presented in the next section for a representative silicone foam.

4. Results for a silicone foam

In this section, the above-derived results for the macroscopic constitutive response and onset of macroscopic instabilities in isotropic closed-cell foams – as characterized by relations (26) and (27) with (28) -- are examined for specific values of the underlying constitutive, geometric, and loading parameters. For comparison with experiments, we take the matrix material to be a typical silicone rubber and hence set $\mu_1 = 0.032$ MPa, $\mu_2 = 0.3$ MPa, $\alpha_1 = 3.837$, and $\alpha_2 = 0.559$, as fitted to the experimental data of Meunier et al. (2008); see Section 2.3 of Lopez-Pamies (2010). Furthermore, we take the environment to be the Earth's atmosphere at sea level and thus set $p_0 = p_{ex} = 1$ Atm $= 0.101$ MPa.

Two types of loading conditions are considered: (i) hydrostatic loading where the macroscopic deformation gradient is given by $\overline{\mathbf{F}} = \overline{\mathbf{F}}_{hy} = \overline{\lambda}\mathbf{I}$, and (ii) uniaxial compression where $\overline{\mathbf{F}} = \overline{\mathbf{F}}_{un} = \mathrm{diag}(\overline{\lambda},\overline{\lambda}_{lat},\overline{\lambda}_{lat})$ with $\overline{\lambda}\leqslant 1$ and the macroscopic Cauchy stress is given by $\overline{\mathbf{T}} = \mathrm{diag}(\overline{t},\overline{t}_{lat},\overline{t}_{lat})$ with $\overline{t}_{lat} = -p_{ex}$. For consistency with standard experimental stress measurements, which are given in terms of force per unit undeformed area of cross section, the results are presented in terms of nominal (or Piola-Kirchhoff) stress measures that are set to be zero at the beginning of the test when $\overline{\mathbf{F}} = \mathbf{I}$. Thus, for the case of hydrostatic loading we utilize the stress measure

$$\overline{S}_{hy} = \mathcal{S}_{11}(\overline{\lambda}\mathbf{I};f_0) + p_{ex} = \mathcal{S}_{22}(\overline{\lambda}\mathbf{I};f_0) + p_{ex} = \mathcal{S}_{33}(\overline{\lambda}\mathbf{I};f_0) + p_{ex}, \tag{31}$$

while for unaxial compression we utilize

$$\overline{S}_{un} = \mathcal{S}_{11}(\overline{\mathbf{F}}_{un};f_0) + p_{ex} \quad\text{and}\quad \overline{S}_{lat} = \mathcal{S}_{22}(\overline{\mathbf{F}}_{un};f_0) + p_{ex}$$
$$= \mathcal{S}_{33}(\overline{\mathbf{F}}_{un};f_0) + p_{ex}, \tag{32}$$

where, again, $\overline{\mathbf{F}} = \overline{\mathbf{F}}_{un} = \mathrm{diag}(\overline{\lambda},\overline{\lambda}_{lat},\overline{\lambda}_{lat})$ with $\overline{\lambda}_{lat}$ being determined by the Cauchy stress condition $\overline{t}_{lat} = \frac{1}{\overline{\lambda}\overline{\lambda}_{lat}}\overline{S}_{22}(\overline{\mathbf{F}}_{un};f_0) = \frac{1}{\overline{\lambda}\overline{\lambda}_{lat}}\overline{S}_{33}(\overline{\mathbf{F}}_{un};f_0) = -p_{ex}$ on the laterals of the specimen.

Fig. 3 shows results for the macroscopic response of the silicone foam with initial porosity $f_0 = 50$, 70, and 90% under hydrostatic loading. Part (a) shows results for compression ($\overline{\lambda}\leqslant 1$) and part (b) for tension ($\overline{\lambda}\geqslant 1$). The corresponding response of a foam with
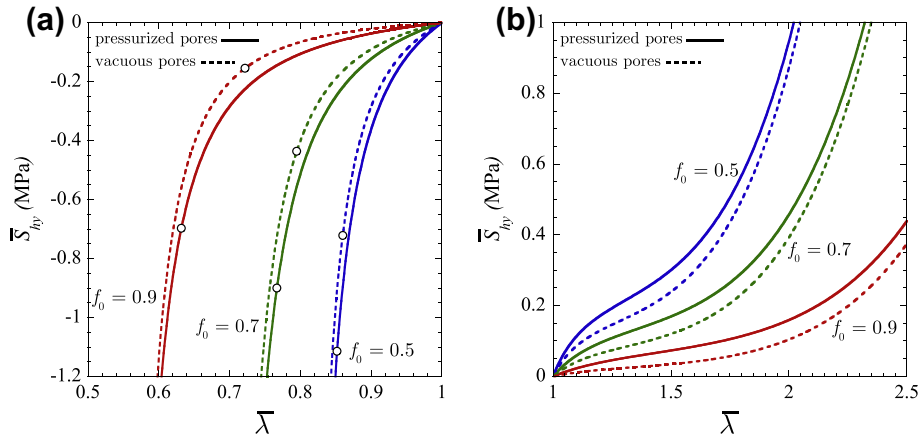
Fig. 3. Macroscopic response of the silicone foam under hydrostatic loading. The results correspond to various values of initial porosity f_0 and are shown in terms of the nominal stress $\overline{S}_{hy}$ as a function of the applied stretch $\overline{\lambda}$. Part (a) displays the results for compression ($\overline{\lambda} \leqslant 1$), and part (b) for tension ($\overline{\lambda} \geqslant 1$). The markers "○" denote the critical states at which the macroscopic response first loses strong ellipticity.
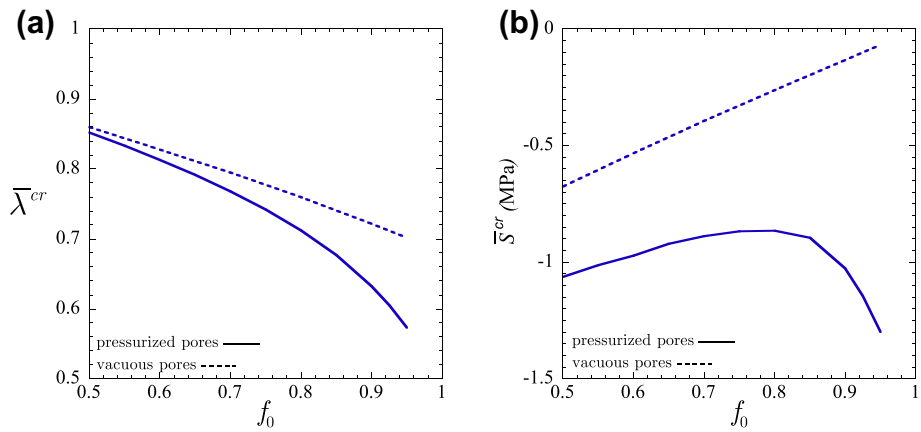

Fig. 4. Critical stretches $\overline{\lambda}^{cr}$ and critical stresses $\overline{S}^{cr}$ at which macroscopic instabilities can first develop in the silicone foam when subjected to hydrostatic compression. The results are shown as functions of the initial porosity f_0.

vacuous pores has also been plotted (dashed lines) for comparison purposes. A first observation from this figure is that the behavior of the foam with pressurized pores is consistently stiffer (both, in compression as well as in tension) than that of the foam with vacuous pores, even for relatively small pressures such as the atmospheric pressure $p_0 = p_{ex} = 0.101$ MPa utilized here. This is

consistent with the fact that the shear modulus of the silicone matrix $\mu = \mu_1 + \mu_2 = 0.332$ MPa in its ground state (similar to the shear modulus of many other standard elastomers) is of the order of the atmospheric pressure.

Another important observation from Fig. 3 is that the presence of internal pore pressure leads to sizably larger critical loads –
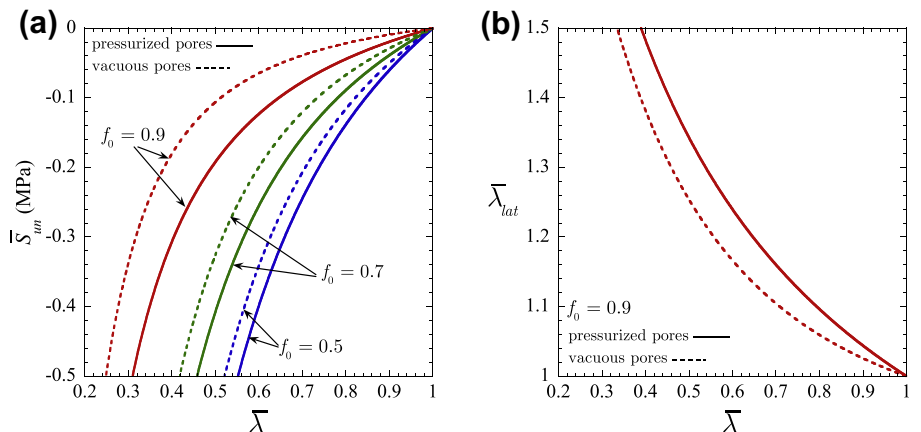

Fig. 5. Macroscopic response of the silicone foam under uniaxial compression for various values of initial porosity f_0. Part (a) shows results for the nominal stress $\overline{S}_{un}$ vs. the applied stretch $\overline{\lambda}$, whereas part (b) shows the lateral stretch $\overline{\lambda}_{lat}$ vs. $\overline{\lambda}$ for the case of $f_0 = 0.9$.

denoted by the symbol "∘" in the plots – at which the foam may develop a macroscopic instability under hydrostatic compression; no instabilities occur under hydrostatic tension. This stabilizing behavior is more clearly illustrated by Fig. 4, where the critical stretches $\bar{\lambda}^{cr}$ and critical stresses $\bar{S}^{cr}$ at which the silicone foam can first become macroscopically unstable when subjected to hydrostatic compression are shown as functions of the initial porosity f_0 (up to a maximum value of $f_0 = 95\%$). Note in particular from these plots that the stabilizing effect of internal pore pressure is consistently more significant for increasing values of initial porosity f_0, in both deformation and stress space.

To further probe the effect of internal pore pressure on the silicone foam, Fig. 5 displays results for its response under uniaxial compression. Plots are shown for the nominal stress $\bar{S}_{un}$ and the lateral stretch $\bar{\lambda}_{lat}$ in terms of the applied stretch $\bar{\lambda}$ for various values of initial porosity f_0. Much like for the preceding case of hydrostatic loading, the response of the foam with pressurized pores is seen to be significantly stiffer than the corresponding response of the foam with vacuous pores. The less compliant deformation in the lateral direction of the pressurized foam shown in part (b) of the figure further supports the general observation that internal pore pressure stiffens the response of the foam. Finally, we note that no instabilities occur under this type of loading conditions, irrespectively of whether the pores are pressurized (see Section 3.1.4 in Lopez-Pamies and Ponte Castañeda, 2007b).

5. Final comments

The results worked out in this paper indicate that the presence of internal pore pressure can significantly alter the macroscopic response and stability of closed-cell elastomeric foams. In particular, foams with internal pore pressure exhibited stiffer and more stable mechanical behaviors than their counterparts with vacuous pores, even for relatively small internal pressures such as atmospheric pressures. At a fundamental level, this behavior can be understood from the fact that the stiffness of elastomers is very low, in the order of the atmospheric pressure.

From a practical point of view, the results also highlight that – as opposed to other types of foams where the matrix material is much stiffer, such as for instance metallic foams – taking into account internal pore pressure, as well as the pressure of the environment, is absolutely necessary in order to be able to accurately predict the mechanical behavior and failure of closed-cell elastomeric foams.

References

Danielsson, M., Parks, D.M., Boyce, M.C., 2004. Constitutive modeling of porous hyperelastic materials. Mech. Mater. 36, 347–358.
Gent, A.N., Tompkins, D.A., 1969. Nucleation and growth of gas bubles in elastomers. J. Appl. Phys. 40, 2520–2525.
Geymonat, G., Müller, S., Triantafyllidis, N., 1993. Homogenization of nonlinearly elastic materials, microscopic bifurcation and macroscopic loss of rank-one convexity. Arch. Rat. Mech. Anal. 122, 231–290.
Hill, R., 1972. On constitutive macro-variables for heterogeneous solids at finite strain. Proc. R. Soc. Lond. A 326, 131–147.
Idiart, M.I., Lopez-Pamies, O., 2012. On the overall response of elastomeric solids with pressurized cavities. Special issue on "Recent Advances in Micromechanics of Materials". C.R. Mec. doi:10.1016/j.crme.2012.02.018.
Lopez-Pamies, O., 2010. A new I_1-based hyperelastic model for rubber elastic materials. C.R. Mec. 338, 3–11.
Lopez-Pamies, O., Ponte Castañeda, P., 2007a. Homogenization-based constitutive models for porous elastomers and implications for macroscopic instabilities: I—Analysis. J. Mech. Phys. Solids 55, 1677–1701.
Lopez-Pamies, O., Ponte Castañeda, P., 2007b. Homogenization-based constitutive models for porous elastomers and implications for macroscopic instabilities: II—Results. J. Mech. Phys. Solids 55, 1702–1728.
Lopez-Pamies, O., Idiart, M.I., 2009. An exact result for the macroscopic response of porous Neo–Hookean solids. J. Elast. 95, 99–105.
Meunier, L., Chagnon, G., Favier, D., Orge, L., Vacher, P., 2008. Mechanical experimental characterisation and numerical modelling of an unfilled silicone rubber. Polym. Test. 27, 765–777.
Michel, J.C., Lopez-Pamies, O., Ponte Castañeda, P., Triantafyllidis, N., 2007. Microscopic and macroscopic instabilities in finitely strained porous elastomers. J. Mech. Phys. Solids 55, 900–938.
Moraleda, J., Segurado, J., Llorca, J., 2007. Finite deformation of porous elastomers: a computational micromechanics approach. Philos. Mag. 87, 5607–5627.
R.W., Ogden, 1997. Non-linear elastic deformations. Dover.
Yamabe, J., Nishimura, S., 2009. Influence of fillers on hydrogen penetration properties and blister fracture of rubber composites for O-ring exposed to high-pressure hydrogen gas. Int. J. Hydrogen Energy 34, 1977–1989.
Yamabe, J., Matsumoto, T., Nishimura, S., 2011. Application of acoustic emission method to detection of internal fracture of sealing rubber material by high-pressure hydrogen decompression. Polym. Test. 30, 76–85.